PHYSICAL REVIEW B **78**, 201408(R) (2008)

Spectromicroscopy of single and multilayer graphene supported by a weakly interacting substrate

Kevin R. Knox,[1,2] Shancai Wang,[2,3] Alberto Morgante,[4,5] Dean Cvetko,[4,6] Andrea Locatelli,[7] Tevfik Onur Mentes,[7] Miguel Angel Niño,[7] Philip Kim,[1] and R. M. Osgood, Jr.[2,*]

[1]*Department of Physics, Columbia University, New York, New York 10027, USA*

[2]*Department of Applied Physics, Columbia University, New York, New York 10027, USA*

[3]*Department of Physics, Renmin University of China, Beijing, People's Republic of China*

[4]*Laboratorio TASC, INFM, Basovizza, Trieste 34012, Italy*

[5]*Department of Physics, Trieste University, Trieste 34127, Italy*

[6]*Faculty for Mathematics and Physics, University of Ljubljana, Ljubljana, Slovenia*

[7]*Elettra–Sincrotrone Trieste S.C.p.A., Basovizza, Trieste 34012, Italy*

(Received 14 October 2008; published 25 November 2008)

We report measurements of the electronic structure and surface morphology of exfoliated graphene on an insulating substrate using angle-resolved photoemission and low-energy electron diffraction. Our results show that, although exfoliated graphene is microscopically corrugated, the valence band retains a massless fermionic dispersion with a Fermi velocity of $\sim 10^6$ m/s. We observe a close relationship between the morphology and electronic structure, which suggests that controlling the interaction between graphene and the supporting substrate is essential for graphene device applications.

DOI: 10.1103/PhysRevB.78.201408 PACS number(s): 79.60.Dp, 61.05.jh, 68.37.Nq, 73.20.At

Since its recent experimental realization,[1] graphene has been the subject of intense research interest primarily because of its unusual electronic transport properties. Its unique conical valence and conduction bands—termed Dirac cones—mimic the dispersion of relativistic massless fermions.[2] This leads to intriguing new transport phenomena—for example, a half integer quantum Hall effect and Berry's phase have recently been discovered in exfoliated graphene.[3,4] However, due to limitations in the size of exfoliated graphene flakes, previous experimental investigations of the valence band of graphene have been carried out on layers grown epitaxially on substrates such as SiC,[5–7] Ni,[8,9] and Ru.[10] Although epitaxial graphene shares many of the same physical properties as exfoliated graphene, it is not a true self-supporting two-dimensional (2D) crystal, but is intrinsically bound to the substrate. Graphene grown on SiC is modified by interaction with the substrate,[11–13] which may have an effect on its measured electronic properties. Additionally, graphene samples grown on SiC are not uniform; rather, they consist of disconnected domains several hundred nanometers in size, each differing in thickness.[11–13] On the other hand, graphene sheets cleaved from bulk graphite are high quality, uniform in thickness, and are true 2D crystals, capable of maintaining crystalline order without a supporting substrate. Exfoliated graphene on SiO_2 is the system of choice for the majority of transport experiments as it is relatively easy to gate and has shown the most interesting electrical transport properties. However, given the small size of currently available samples, microscopic probing techniques are required to study these sheets. Here, we report measurements of the surface morphology and electronic structure of exfoliated graphene on SiO_2 using microspot low-energy electron diffraction (μLEED) and microspot angle-resolved photoemission spectroscopy (μARPES). Our diffraction measurements show that monolayer and multilayer graphene sheets are not atomically flat, but microscopically corrugated. Our photoemission measurements confirm that the electronic dispersion is linear in the vicinity of the Dirac point with a Fermi velocity of $\sim 10^6$ m/s.

Graphene samples were extracted by micromechanical cleavage from Kish graphite crystals (Toshiba Ceramics, Inc.) and placed onto a SiO_2 on Si substrate as described in Ref. 1. Graphene sheets with lateral sizes as large as 50 μm were placed in contact with Au grounding stripes via thermal deposition through a metal shadow mask. The graphene layers were characterized with low-energy electron microscopy (LEEM) before investigation with μARPES and μLEED. The experiments were performed in UHV conditions at the Nanospectroscopy beamline in use at the Elettra Synchrotron facility in Trieste, Italy. This instrument reaches a lateral resolution of less than 40 nm in imaging modes. Momentum and energy resolution for μARPES experiments were 0.019 $Å^{-1}$ and 300 meV, respectively, at incident photon energies of 90 and 84 eV. μARPES and μLEED measurements were restricted to regions of 2 μm in diameter. X-ray photoemission electron microscopy (XPEEM) with 403-eV photons was employed to examine the graphene sheets for impurities that may have been introduced in the preparation procedure. Traces of Au contamination were identified only in the immediate proximity (<5 μm) of the Au stripes (see Fig. 1). All μLEED and μARPES experiments were restricted to areas of graphene that were not contaminated by Au deposition.

LEEM was used to locate sample areas of interest and determine film thickness. Figure 1 compares optical microscopy and LEEM images of a typical sample. The gray bands in the LEEM image correspond to graphene regions of different layer thickness. The observed difference in contrast is due to a quantum-size effect resulting from the interference between electron waves scattered at the surface and at the interface with the substrate. The positions and number of the maxima and minima in the electron reflectivity as a function of electron energy allow the identification of the exact film thickness[13–16] (details will be presented elsewhere). The

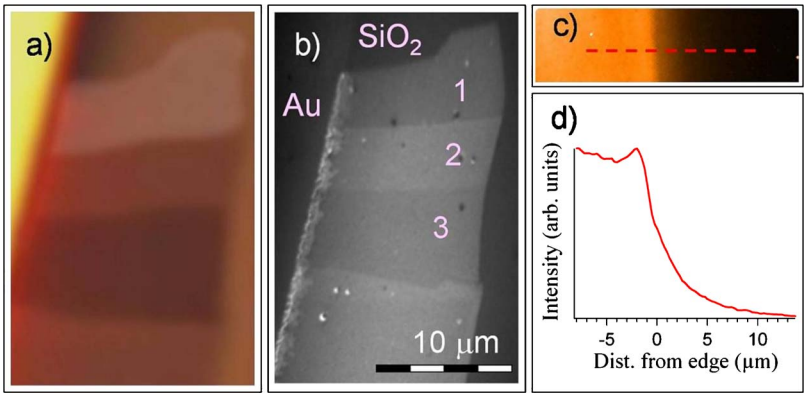

FIG. 1. (Color online) (a) Optical microscopy image of monolayer and multilayer graphene samples (contrast enhanced). (b) LEEM image of the same sample. Numbers indicate graphene thickness in monolayers (ML). (c) XPEEM image of Au 4*f* 7/2 core level taken at edge of Au wire on graphene. (d) Intensity profile along red dashed line in (c).

sample-layer thickness was independently confirmed by micro-Raman measurements.[17–19]

The crystalline structure of the samples was investigated using μLEED. As shown in Fig. 2, the Gaussian width of the primary and secondary μLEED peaks increases with decreasing film thickness, reaching a maximum for monolayer graphene. A natural explanation for this phenomenon is that thin graphene sheets conform to an undulating SiO_2 surface, while thicker sheets are stiffer and less likely to follow the contours of the substrate. Additionally, we note that the width of the diffraction spots increases linearly with k [see Fig. 2(f)], where k is the total momentum of μLEED electrons, related to incident electron energy by $k=\sqrt{2m_eE_{\mathrm{kin}}}$. This implies a constant angular spread in the direction of reflected μLEED electrons, which is further evidence to suggest that the surface of the graphene layers is microscopically corrugated. Point defects such as missing carbon atoms or contaminants adsorbed on the graphene surface would not produce such broadening of the μLEED peaks, while structural defects that divide regions shifted by fractional lattice vectors would result in broad μLEED spots with typical nonmonotonic electron energy dependence (in contrast with our observations). If we make the simplifying assumptions that the corrugation of the graphene sheets is random and that the length scale of the ripples is larger than the transfer width of our μLEED apparatus, we may model our data as an incoherent sum of μLEED intensities over multiple domains with different local surface normals. Assuming a Gaussian distribution for the local surface normal, the standard deviation, $\Delta\theta_{\mathrm{norm}}$, can be readily obtained using a simple trigonometric relation,

$$\Delta\theta_{\mathrm{norm}} \approx \frac{1}{2}\frac{\hbar\Delta k_{\parallel}}{\sqrt{2m_eE_{\mathrm{kin}}}}, \tag{1}$$

where $\Delta k_{\parallel}$ is the Gaussian width of the central diffraction maximum. Application of the above formula to the μLEED peaks shown in Fig. 2(e) results in a $\Delta\theta_{\mathrm{norm}}$ of $6.1^\circ \pm 0.5^\circ$ for monolayer graphene and $2.4^\circ \pm 0.5^\circ$ and $1.7^\circ \pm 0.5^\circ$ for bilayer and trilayer graphene, respectively. These results are in accord with measurements of the same quantity by scanning tunneling microscopy and electron diffraction,[20–23] as well as recent transport measurements, which indicate that ripples in graphene samples supported by SiO_2 play a significant role in transport properties.[24]

In the standard tight-binding model, the theoretical dispersion of graphene valence-band electrons is given by[25]

$$E(\mathbf{k}) = -t\sqrt{1+4\cos(\sqrt{3}ak_y/2)\cos(ak_x/2)+4\cos^2(ak_x/2)}, \tag{2}$$

where t is the nearest-neighbor hopping energy and a is the lattice constant. This equation yields a nearly linear dispersion relation in the vicinity of E_F—electrons mimic massless particles, traveling at a fixed speed of $\sim 10^6$ m/s. μARPES directly probes this dispersion. We collected μARPES data from graphite flakes and monolayer graphene sheets over the first Brillouin zone from 1 to −10 eV (referenced to E_F). The angle-integrated graphene and graphite spectra are shown in Fig. 3(a). Comparing the two we note that, although the overall features are similar, the graphene spectrum is shifted toward higher binding energy by ~300 meV, an effect that we attribute to charging of the SiO_2 substrate by photoionization from the incident UV beam.

Angle-resolved graphite and graphene spectra are shown in Figs. 3(b) and 3(c), respectively, for three principal Brillouin-zone directions: ΓM, MK, and KΓ. The angle-resolved graphite spectrum is in accord with prior measure-

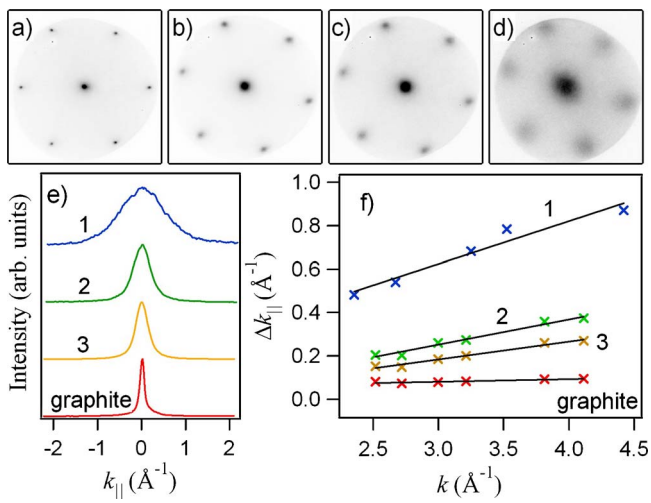

FIG. 2. (Color online) (a)–(d) Graphite, trilayer, bilayer, and monolayer graphene μLEED patterns at 42 eV, respectively. (e) Intensity profiles of central diffraction maximum from (a)–(d). Numbers indicate thickness in ML. (f) Gaussian width of central diffraction maxima as a function of k.

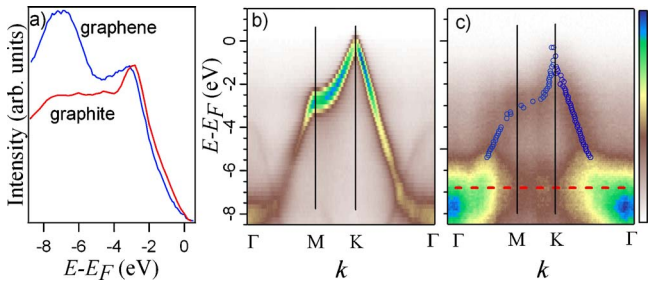

FIG. 3. (Color online) (a) Angle-integrated photoemission intensity for graphite (red) and graphene (blue). (b),(c) μARPES intensity along principal Brillouin-zone directions for graphite and graphene, respectively. $h\nu$=90 eV. Blue circles in (b) represent peak positions obtained from Gaussian fits to MDCs. (Brillouin-zone symmetry-point labels are valid for a 2D approximation of the graphite Brillouin zone.)

ments of the graphite band structure.[26,27] The degraded appearance of the angle-resolved monolayer spectrum is due, primarily, to the undulations of the graphene layer, which produce broader photoemission features than the atomically flat graphite flakes. Additionally, the monolayer graphene film is nearly transparent to UV photons and SiO_2-emitted photoelectrons at these energies.[28] Thus, our measured graphene photoemission spectrum contains a nondispersive SiO_2 peak at −7 eV; this feature is in accord with previous measurements of the amorphous SiO_2 band structure.[29] Despite the relatively large width of the photoemission features and the presence of SiO_2 photoelectrons, we are able to map out accurately the monolayer dispersion within 5 eV of the Fermi level due to the large band gap of the SiO_2 substrate. For each of the three principal Brillouin-zone directions noted above we obtained momentum distribution curves (MDCs) at 100-meV intervals. These were each fit with a single Gaussian peak with a maximum uncertainty in position of 0.015 Å^{-1}. The peak positions are indicated by blue circles in Fig. 3(c).

In addition, MDCs taken along principal Brillouin-zone directions passing through the K point for both graphite and graphene are shown in Fig. 4. For the case of graphite, we display the negative second derivative (to enhance the intensity of the peaks) of a spectrum taken vertically through the K point. In this case the photon energy was adjusted to 84 eV, which results in a perpendicular momentum of $k_z \approx 0.05\ \text{c}^*$ within the graphite bulk, where c^* is the graphite reciprocal-lattice vector associated with the perpendicular direction (k_z was calculated using the standard free-electron approximation of the μARPES final state[30]). At this k_z, we access the K point of the three-dimensional (3D) graphite Brillouin zone, which allows us to resolve the parallel dispersing branches representing the split π band associated with the two inequivalent graphite sublattices. In contrast, the graphene MDCs did not display any dependence on photon energy and were always well fit by a single peak, as expected, since a monolayer graphitic lattice is expected to have a degenerate spectrum with only one dispersing peak. The graphene spectrum shown in Fig. 4(c) was taken in the horizontal or ΓK direction through the K point. In this direction only a single dispersing branch of the Dirac cone is

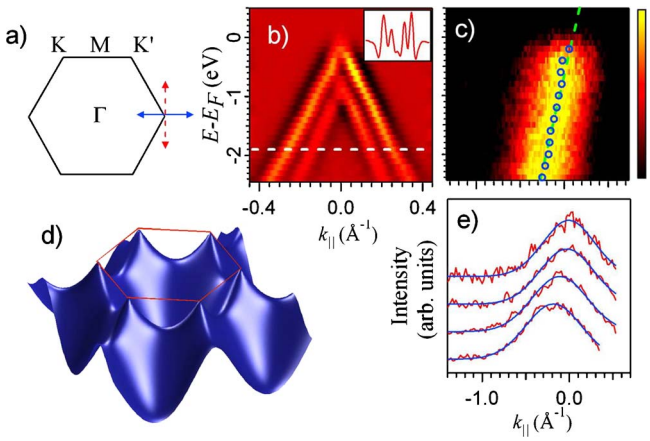

FIG. 4. (Color online) (a) 2D graphite/graphene Brillouin zone, red dotted arrows, and blue solid arrows indicate vertical and horizontal directions through K point, respectively. (b) Negative second derivative of graphite μARPES intensity through K point along vertical direction. $h\nu$=84 eV. Inset shows intensity along dotted white line. (c) Graphene μARPES intensity through K point along horizontal direction. $h\nu$=90 eV. All MDCs have been normalized to the same height. Blue circles represent peak positions from MDC fits. Dotted green line represents theoretical Fermi velocity. (d) Theoretical valence-band dispersion of graphene using Eq. (2). Red lines indicate first Brillouin-zone boundary. (e) Red lines represent MDCs taken from above graph. Blue lines represent best fit Gaussian peaks. (Note: All parallel momenta are referenced to K point.)

visible due to a photoemission interference effect.[27]

Note that the graphene MDCs are significantly wider than the graphite MDCs. In conventional ARPES as well as μARPES experiments, the MDC width can normally be related to the imaginary part of the complex self-energy, $\text{Im}[\Sigma(\mathbf{k})]$, of charge carriers in the crystal.[31–33] However, in our experiment there are contributions to MDC width that are unrelated to $\text{Im}[\Sigma(\mathbf{k})]$. The first is interaction with charged impurities in the SiO_2 substrate, which results in a local shift in the chemical potential of the graphene sheet—an excess of electrons or holes often called a "charge puddle."[34,35] Since the lateral scale of these puddles is ~100 nm,[35] our photoemission results (collected over ~2 μm) average over many such fluctuations, causing a broadening in energy space of our photoemission features. The corresponding broadening in k space is then given by $\Delta k_\parallel = \Delta E/\hbar v_F$. ΔE is estimated to be ~100 meV (Refs. 34 and 35); from this we obtain $\Delta k_\parallel = 0.015\ \text{Å}^{-1}$, which is a small contribution to the total MDC width of 0.47 Å^{-1}.

However, undulations on the graphene surface are responsible for the majority of MDC broadening. As with our μLEED results, our μARPES measurements sample many tilted domains since the characteristic length scale for the ripples is two orders of magnitude smaller (~10 nm) (Ref. 22) than our photoemission region (~2 μm). Although the electron phase coherence length in graphene is expected to be longer than the length scale for surface undulations, we will again model our μARPES results as an incoherent sum over multiple domains and use Eq. (1) to estimate $\Delta\theta_{\text{norm}}$ from the spread in $k_\parallel$. For electrons photoemitted from the Fermi level $E_{\text{kin}} \approx 86$ eV and the fits in Fig. 4(e) provide

$\Delta k_{\|}=0.47\pm0.03$ Å^{-1}, which yields $\Delta\theta_{\text{norm}}=3°$. This value for $\Delta\theta_{\text{norm}}$ is comparable to, although smaller than, that calculated from the μLEED data. The discrepancy is likely due to the simplifying assumption that μARPES intensities from multiple tilted domains add incoherently.

Despite the broadening of photoemission features described above, it is possible to measure accurately the electronic dispersion near the *K* point and determine the Fermi velocity. Graphene MDCs taken at regular energy intervals in the horizontal direction were fit with a single Gaussian peak [see Fig. 4(e)]. With no constraints on the fitting parameters, the uncertainty in the position of the peaks was less than 0.006 Å^{-1} and the uncertainty in width was less than 0.01 Å^{-1}. Additionally, the width in momentum space was very consistent from peak to peak, independent of energy (0.47 ± 0.03 Å^{-1}). In the vertical direction through the *K* point, we observed two symmetric dispersing peaks, as expected. However, since the separation between peaks in the vertical direction was small compared to the total width of the individual peaks (also $\sim$0.5 Å^{-1}), analysis of the dispersion in the horizontal direction, where only a single dispersing peak is observed, is the most straightforward way to determine the Fermi velocity. Since our μARPES system measures the entire first Brillouin zone a single scan contains information about all six Dirac points in the first zone. Averaging the results from all *K* points we obtain a measured Fermi velocity of $1.09\pm0.15\times10^6$ m/s, in very good agreement with the theoretical prediction.

In summary, we have used spectromicroscopy to probe the surface morphology and electronic structure of exfoliated single-layer and multilayer graphene on a micron scale. Our μLEED results show that the characteristic graphite hexagonal lattice structure is maintained up to the single layer. However, electron diffraction is degraded by undulations of the graphene surface. An estimate of the standard deviation of the surface normal can be obtained from an analysis of the μLEED data—our result is comparable to recent measurements of the same quantity.[20–24] Photoemission measurement of the valence band of monolayer graphene is possible due to the large band gap of the SiO_2 substrate. The MDC widths of graphene peaks are larger than those of comparable features on graphite, an effect that is attributed to undulations of the graphene layer. Nonetheless, an accurate measurement of the electronic dispersion near E_F is possible. Our data show clearly that the band structure of exfoliated graphene is well described by the standard one-orbital tight-binding model, which predicts a linear dispersion relationship near the *K* point. A greater theoretical understanding will be necessary to extract $\text{Im}[\Sigma(\mathbf{k})]$ from the MDC widths as undulations of the graphene layer obscure this quantity. Additionally, further experimental work will be necessary to understand the effect of the SiO_2 substrate on these undulations.

R.O. acknowledges support from the DOE under Contract No. DE-FG02-04-ER-46157; K.K., P.K, and S.W. acknowledge support from the NSF under Award No. CHE-0641523 and NYSTAR, and A.M., D.C., A.L., T.M., and M.N. from MIUR-PRIN2006 under Project No. 2006020543_002. S.W. acknowledges support from the National Basic Research Program of China under Award No. 2007CB925001. The authors would also like to thank Andrew Millis, Jerry Dadap, and Mehmet Yilmaz for valuable discussions.

*osgood@columbia.edu

[1] K. S. Novoselov *et al.*, Science **306**, 666 (2004).
[2] D. P. DiVincenzo and E. J. Mele, Phys. Rev. B **29**, 1685 (1984).
[3] K. S. Novoselov *et al.*, Nature (London) **438**, 197 (2005).
[4] Y. B. Zhang *et al.*, Nature (London) **438**, 201 (2005).
[5] T. Ohta *et al.*, Science **313**, 951 (2006).
[6] A. Bostwick *et al.*, Nat. Phys. **3**, 36 (2007).
[7] S. Y. Zhou *et al.*, Nat. Phys. **2**, 595 (2006).
[8] Yu. S. Dedkov *et al.*, Phys. Rev. Lett. **100**, 107602 (2008).
[9] A. M. Shikin *et al.*, Phys. Rev. B **62**, 13202 (2000).
[10] A. L. Vázquez de Parga *et al.*, Phys. Rev. Lett. **100**, 056807 (2008).
[11] I. Forbeaux *et al.*, Phys. Rev. B **58**, 16396 (1998).
[12] C. Berger *et al.*, J. Phys. Chem. B **108**, 19912 (2004).
[13] H. Hibino *et al.*, Phys. Rev. B **77**, 075413 (2008).
[14] M. S. Altman, J. Phys.: Condens. Matter **17**, S1305 (2005).
[15] K. L. Man *et al.*, Phys. Rev. Lett. **93**, 236104 (2004).
[16] T. Ohta *et al.*, New J. Phys. **10**, 023034 (2008).
[17] A. C. Ferrari *et al.*, Phys. Rev. Lett. **97**, 187401 (2006).
[18] A. Gupta *et al.*, Nano Lett. **6**, 2667 (2006).
[19] D. Graf *et al.*, Nano Lett. **7**, 238 (2007).
[20] J. C. Meyer *et al.*, Nature (London) **446**, 60 (2007).
[21] A. Fasolino *et al.*, Nature Mater. **6**, 858 (2007).
[22] E. Stolyarova *et al.*, Proc. Natl. Acad. Sci. U.S.A. **104**, 9209 (2007).
[23] M. Ishigami *et al.*, Nano Lett. **7**, 1643 (2007).
[24] S. V. Morozov *et al.*, Phys. Rev. Lett. **97**, 016801 (2006).
[25] P. R. Wallace, Phys. Rev. **71**, 622 (1947).
[26] K. Sugawara *et al.*, Phys. Rev. B **73**, 045124 (2006).
[27] E. L. Shirley *et al.*, Phys. Rev. B **51**, 13614 (1995).
[28] M. P. Seah and W. A. Dench, Surf. Interface Anal. **1**, 2 (1979).
[29] T. H. DiStefano and D. E. Eastman, Phys. Rev. Lett. **27**, 1560 (1971).
[30] S. Hüfner, *Photoelectron Spectroscopy* (Springer, Berlin, 1995).
[31] A. Kaminski and H. M. Fretwell, New J. Phys. **7**, 98 (2005).
[32] A. A. Kordyuk *et al.*, Phys. Rev. B **71**, 214513 (2005).
[33] N. M. R. Peres *et al.*, Phys. Rev. B **73**, 125411 (2006).
[34] J. Martin *et al.*, Nat. Phys. **4**, 144 (2008).
[35] V. M. Galitski *et al.*, Phys. Rev. B **76**, 245405 (2007).